FORESTCAST: FORECASTING DEFORESTATION RISK AT SCALE WITH DEEP LEARNING

Matthew Overlan*[1], Charlotte Stanton[2], Maxim Neumann[1], Arianna Manzini[1], Julia Haas[1], Michelangelo Conserva[2], Mélanie Rey[1], Kira Prabhu[3], Youngin Shin[3], Kuan Lu[3], and Drew Purves[1]

[1]Google DeepMind
[2]Google Research
[3]Google

ABSTRACT

Deforestation is a major threat to biodiversity and the stability of the climate. Current monitoring solutions provide reactive alerts only after deforestation has occurred, rendering them inadequate for prevention. Proactive deforestation prevention necessitates forecasting at-risk areas; however, previous forecasting efforts have been constrained by their reliance on simple statistical models and limited feature sets. This paper introduces the ForestCast dataset, the first publicly available dataset dedicated to training deep learning models for the task of deforestation risk forecasting. We benchmark several deep learning models from the literature, as well as a Random Forest Decision Tree model, and find that the deep learning models perform the best. Furthermore, we test the relative importance of three classes of input data: 1) satellite imagery, 2) derived feature layers such as slope and distance to roads, and 3) change history, an image summarizing past deforestation. We find that change history is important, but the most flexible models perform well with satellite imagery (or embeddings derived from imagery) alone. Lastly, we present a preliminary assessment of the ethics of using deforestation risk models in practice.

1 INTRODUCTION

Deforestation poses a critical threat to global biodiversity and climate stability, with total tropical primary forest loss in 2024 reaching 6.7 million hectares—equivalent to almost 18 football (soccer) fields of forest lost every minute (Weisse et al., 2024). This loss not only endangers countless species but also disrupts vital ecosystem services, including carbon sequestration and water regulation (Daily et al., 1997). Indeed, forests play an essential role in sustaining livelihoods, particularly in tropical regions where many communities depend on these ecosystems for their survival and economic prosperity (IPBES, 2019; Food and Agriculture Organization, 2014).

Much of the devastation inflicted on forests is driven by unsustainable business practices, including agricultural expansion, logging, and infrastructure development. These activities have drawn increasing scrutiny from investors (Holder, 2021) and regulators (Schröder, 2022) alike, prompting calls for improved environmental performance from companies across various sectors. The European Union Deforestation Regulation (EUDR, European Commission: Directorate-General for Environment (2023); European Union (2023)) exemplifies this shift, by curbing the import of products linked to deforestation and requiring companies to demonstrate compliance with sustainable sourcing practices. In turn, businesses are adapting to a landscape where environmental stewardship is no longer optional but a prerequisite for market participation.

To effectively navigate these changes, the ability to predict deforestation trends is paramount. Forecasting high-risk areas would enable companies to proactively manage their supply chains, mitigating potential

*The authors wish to thank Alex Wilson, Michal Kazmierski, Chris Brown, Valerie Pasquarella, Alexis Boukouvalas, Sophia Alj, Maria Abi Raad, Ben Bariach, Dan Morris, Gena Gibson, Henry Glick, Andrew Wilcox, Michael Marano, and Tracey Osborne for helpful discussions and other contributions to this work.

disruptions and aligning their operations with sustainability goals. Such foresight would not only benefit corporations but also non-governmental organizations dedicated to conservation efforts. Equipping NGOs with predictive insights would empower them to target interventions more effectively, safeguarding forests before they fall victim to irreversible damage. Moreover, for indigenous peoples and local communities, predictive models could serve as tools for advocacy and empowerment. By providing early warnings of potential deforestation, forecasts could help communities mobilize and take action to protect their ancestral lands and resources.

Finally, deforestation risk forecasting can also enhance the integrity and effectiveness of conservation investments. Assessing the additionality of such investments — demonstrating that conservation outcomes would not have occurred without a given intervention — is a critical challenge. Predictive models like the one presented here can provide a baseline of likely deforestation in the absence of an intervention, allowing for a more robust evaluation of its potential impact. Notably, carbon credit standard-setting organizations have started integrating deforestation risk probabilities into their methodologies to provide a more rigorous framework for assessing the impact of avoided deforestation projects (Verra, 2023; 2024). This integration underscores the recognition of predictive modeling as an essential tool for increasing the credibility and effectiveness of conservation finance.

This manuscript explores the potential of deep learning to forecast deforestation risk, shifting from reactive monitoring to proactive prevention. To address the needs of governments, NGOs and actors in the private sector, we leverage large-scale satellite imagery and the latest computer vision AI models, to create a deforestation risk methodology that is:

- **Accurate**, in that the model predictions are at least as accurate as previous models, most of which rely only locally specific features such as roads and / or statistical (non deep learning) models. We demonstrate this by evaluating several models and model-types across two label sources and using multiple metrics, as well as assessing the relative contribution of three classes of input features to better understand the drivers of model performance.
- **Trustworthy**, in that we compare the relative importance of three classes of input features to better understand the drivers of model performance, and we measure performance on two distinct sources of ground truth data. These novel evaluations strengthen trust that the final model is as accurate as it can be.
- **Consistent**, in that the same machine learning model, with the same approach to training data, inputs, evaluation, can be used anywhere, allowing for meaningful comparisons across regions. We achieve this by using global, satellite-derived training and inputs only.
- **Future Proof**, in that we can be confident that the model inputs will be refreshed in future years, allowing for updated calculations of risk, and meaningful comparison across years. Our satellite-imagery based model achieves this because the satellite-derived inputs can be expected to be made available every year for the foreseeable future.
- **Scalable**, in that the methodology is sufficiently computationally efficient to run at high resolution over large regions, potentially all the way to global. We achieve this by using recent deep learning vision models that work tile-to-tile rather than pixel-to-pixel or tile-to-pixel (i.e. they take in a grid of pixels, and output a grid of pixels).
- **Verifiable and Transparent**, in that the research community can repeat and build on our work. We achieve this by releasing the training and evaluation data used in this manuscript as a machine learning benchmark.

2 Prior Work

Several previous works have considered the problem of deforestation risk forecasting, using a variety of methods and data sources. We survey several relevant machine learning-based works here, noting that there is an earlier literature based on other methods (Rosa et al., 2013). Together, these machine learning studies prove that it is sometimes possible to predict deforestation risk to a high accuracy at local scales. However,

these methods do not meet all of the criteria listed above. Most studies rely on combinations of locally-tailored approaches to training data; and / or local specialized input features that are not available everywhere, and that may quickly go out of date. Thus, they are not consistent or future proof. Furthermore, most of the models have not released their training and input data, which hampers verifiability and transparency.

Our work is most similar to that of Ball et al. (2022) who used deforestation labels from the Global Forest Change dataset from Global Forest Watch (GFW-GFC) (Hansen et al., 2013), and trained on the composite satellite images included in that dataset for two regions in the Peruvian Amazon. They evaluated several convolutional neural networks, achieving good results particularly with the 3D CNN. While Ball et al. uses globally available training and input data, it utilizes a model that is hard to scale to large regions because it works tile-to-pixel, and hence requires a costly moving window approach to predict for large regions. Moreover, Ball et al. (in common with other works) have not ablated input data to compare their relative importance, and they have not released their training dataset, making it hard to repeat or build on the work.

Engelmann & Toetzke (2023) also used deep convolutional models (UNet and ResUNet), using MAPBIOMAS data (Souza et al., 2020) for input and labels over the Brazilian Amazon, but were unable to achieve good scores until coarsening the task to predict tile-level deforestation rates.

Another recent work leveraging a deep learning model is Goldman et al., which used Land Change Modeler (Eastman & Toledano, 2018) to predict labels from GFW-GFC using a suite of features including forest cover and forest loss from GFC, distance to roads, land cover, protected areas, concessions data, and more. The proprietary Land Change Modeler from Clark Labs is a software tool for modeling land cover change. It provides an interface for training models (such as Multi-layer Perceptron and logistic regression) to predict the probability of land cover transitions given explanatory variables provided by the user. The trained model can then be used to simulate future transition quantity and spatial distribution. They reported high accuracies for several areas in the Democratic Republic of Congo.

Works utilizing statistical (non deep learning) models, include Jaffé et al. (2021), which used a Bayesian hierarchical spatial model to forecast deforestation in the Brazilian Amazon, using MAPBIOMAS data for labels and 20 input variables such as distance to urban areas, distance to roads, GDP, and forest edge density. Sales et al. (2017) used highly modified Generalized Linear Models (to account for spatial correlation, for example) to model deforestation in the Brazilian Amazon, using PRODES (National Institute For Space Research) data as labels and similar input features as above. Sboui et al. (2023) created their own deforestation labels for northern Sumatra, Indonesia using NDVI (which is derived from satellite data), and trained a random forest model based on variables such as distance to roads and rivers. van Stokkom et al. (2020) created their own deforestation labels for an area in Borneo, Indonesia using Sentinel 1 satellite data. They then found that gradient-boosted decision trees gave the best results on their data.

Vieilledent et al. (2023) modeled deforestation risk over the entire tropics, the only prior work to our knowledge to do so. They used deforestation data from Vancutsem et al. (2021) as labels, and six input features such as distance to roads, etc. They trained three pixel-to-pixel models and found that their spatially-augmented logistic regression performed the best.

A final note is that at time of writing, the approach to deforestation risk modeling with the greatest uptake in practice appears to be the Forest Loss Risk Index (FLRI) (Satelligence, 2022). This is a non-learned model, i.e. a heuristic, that assumes risk is linearly related to distance from previous deforestation in both space and time. The fact that the FLRI is currently the default choice for most practitioners suggests that machine-learning based approaches to deforestation risk have not yet matured to the point where they are considered sufficient to guide decision makers worldwide.

3 METHODS

3.1 HISTORICAL DEFORESTATION DATASET

Despite these prior works, there is not yet a standard dataset and benchmark for predicting future deforestation. Recently released aggregated datasets for large geospatial model training such as FoMo-Bench (Bountos et al., 2023) and GEO-Bench (Lacoste et al., 2023) do not include any temporal forest datasets. We hope that

by describing our dataset and releasing it publicly, it can become a resource that other researchers can use to accelerate progress on this important task.

Our dataset is designed to train deforestation risk forecasting models for fixed time intervals. The dataset and results here are bounded by the tropics, but our methods and data sources are globally applicable.

3.1.1 LABELS

To create a historical deforestation dataset with both global spatial coverage and deep historical temporal coverage, we used algorithmically derived deforestation events as our ground truth labels. This bypasses the need for costly human annotation, at the possible expense of accuracy. We evaluate on two sources of target data made available to the community by others: the Global Forest Change dataset (Hansen et al., 2013), a widely used product which has been providing deforestation monitoring and alerts since 2012; and the Continuous Change Detection and Classification (CCDC) algorithm (Zhu & Woodcock, 2014).

The GFW-GFC annual change maps were produced by extracting a time series of spectral features from Landsat 7 imagery and then training a bagged decision tree classifier to classify pixels as changed or unchanged.

The CCDC algorithm operates on single-pixel time series and fits a variable number of breakpoints that best identify sharp changes in the luminance values of that time series. When applied to forested areas, it fairly reliably identifies forest to non-forest transitions. Our CCDC data were generated using Google Earth Engine's `ee.Algorithms.TemporalSegmentation.Ccdc` algorithm over Landsat data from 2000-2023 (inclusive) (Gorelick et al., 2023). To create labels that can act as a prediction target, we created a mask indicating for every pixel whether a segment ended (as indicated by the `tEnd` band) during the forecast time interval.

Regardless of the source of target labels, we use the GFW-GFC dataset to mask out all non-forest areas, defined as pixels that were either non-forest prior to 2000 (`treecover2000` band $< 25\%$) or have experienced a loss event before the start of the forecast time interval.

These two algorithms yield qualitatively and quantitatively different change masks, so it is important to acknowledge that the quality of any risk forecast is constrained by the quality of the associated training labels.

3.1.2 INPUT DATA

To predict these deforestation events, we constructed a historical deforestation dataset based on satellite time series features. This is in contrast to previous work on deforestation risk forecasting which uses static features derived from satellite imagery and other sources, such as proximity to roads, or composite satellite imagery, as described in Section 2.

Our dataset includes several different sources, enabling us to compare the effectiveness of different input features. We include three sources of satellite imagery, 1) a dense time-series (containing all images within the year prior to the forecast date), 2) annual composites dating back to 2014, and 3) two years of annual geospatial embeddings from Brown et al. (2025). These embeddings are a learned featurization of raw observation data, trained in an unsupervised fashion on a large scale dataset that includes imagery, LIDAR data, and even localized text from Wikipedia. The resulting general-purpose 64-dimensional annual images can be used alongside, or in lieu of, raw observation data for training downstream models like ours.

Satellite imagery is augmented with auxiliary data layers showing mostly static information, such as elevation, distance to roads, etc. The full list of auxiliary data sources is shown in Table 1.

Finally, we include a record of past change for each pixel showing how long ago in years that pixel was deforested, along with a binary mask showing which pixels have experienced deforestation. This change-history layer corresponds to the data source used for the segmentation label (GFW-GFC or CCDC).

All data were downloaded from the Earth Engine Data Catalog (Gorelick et al., 2017) except for GRIP and GWL which were downloaded from the GEE Community Catalog (Roy et al., 2024). All images were resampled to a resolution of 30m/pixel to match the resolution of the GFW-GFC labels.

Table 1: Data sources included in the ForestCast dataset and their preprocessing.

Dataset	Source	Bands Included	Description	Preprocessing
Sentinel 2 L1C	ESA (Copernicus, 2025)	`B2` (Blue), `B3` (Green), `B4` (Red), `B8` (NIR), `B11` (SWIR)	Multi-spectral satellite imagery (10m, ∼5–10 day revisit time)	Log transform pixel values via $\log_{10}(x+1)$, then normalize each band by its dataset mean and standard deviation.
Global Forest Change	GFW (Hansen et al., 2013)	`treecover2000`, `lossyear`, `datamask`	Historical deforestation (30m, annual), tree cover, permanent water, and annual Landsat composite images	Construct a binary water mask from the `datamask` band.
CCDC	Google (Gorelick et al., 2023)	`tEnd`	Historical land change	None
World Database on Protected Areas	UNEP-WCMC, Protected Planet (UNEP-WCMC and IUCN, 2024)	N/A	Protected area boundaries	Construct a binary mask showing whether a pixel is inside of a polygon (of any type).
Gridded Population of the World	NASA SEDAC (CIESIN, 2017)	`population_density`	Population density	Log transform then normalize with $\mu = 3.0$ and $\sigma = 1.0$.
SRTM / NASADEM Digital Elevation	NASA/CGIAR (NASA JPL, 2020; Simard et al., 2024)	`elevation`	Elevation above sea level in meters	Convert elevation to slope as the local gradient using the 4-connected neighbors, then convert to radians.
Oil Palm Plantation	Forest Data Partnership (Forest Data Partnership, 2025)	`probability`	Palm plantation	None
CloudScore+	Google (Pasquarella et al., 2023)	`cs`	Cloud mask	None
Global Roads Inventory Project	GLOBIO (Meijer et al., 2018)	`roads`	Roads	Compute distance to the nearest road in meters, clipped at 5000, then divided by 5000.
Global Mangrove Distribution	ORNL DAAC (Simard et al., 2019)	`agb`	Mangroves & wetlands	None
Global Wetland FC System	Zhang et al. (2023)	`b1`	Wetlands	Convert to binary mask indicating a non-zero value of any category.
AlphaEarth V1	Google (Brown et al., 2025)	`A00` through `A63`	64-band learned geospatial embedding	None

3.1.3 TEMPORAL COVERAGE

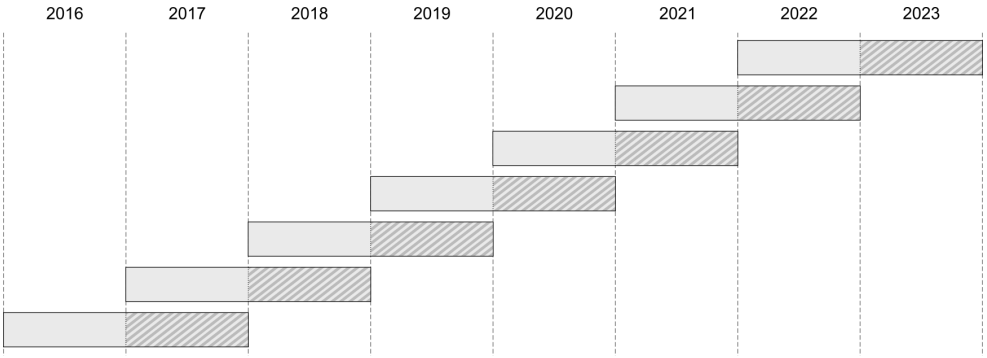

Figure 1: Temporal splits for Sentinel-2 imagery. Each temporal split contains deforestation labels (indicated by the shaded areas), plus one year of Sentinel-2 satellite imagery and auxiliary data for the preceding year. The input data variants using embeddings and GFW-GFC imagery are similar, but with temporally longer input contexts (2 years and 9 years, respectively).

To train our model, we constructed historical data by dividing the satellite imagery and other temporal data into several temporal splits. Each split contains all data sources from Table 1, Sentinel 2 imagery covering one year prior to the label year, and embeddings covering two years, and annual composite imagery from GFW going back to 2014 (the earliest year available in the Earth Engine data catalog). This is combined with records of historical deforestation from both GFW-GFC and CCDC, from which we derive the change history and the labels for that year (Figure 1).

At training time we aggregate data from all splits prior to the year we wish to forecast. For example, if we wish to generate forecasts for 2023, we train the model on all splits from 2022 and before. In this way, we simulate the situation where a model is trained on all available historical data up to the end of one year, then used to forecast the risk of deforestation during the next year. While we only evaluate annual risk forecasts, the model and data could be adapted to allow for predictions more than one year in advance.

3.1.4 SPATIAL COVERAGE

We constructed our dataset by first sampling many points over the forested areas of the tropics (Figure 2), and then constructing training examples for each point.

To sample points, we first construct a covering grid of size 7680m^2, which corresponds to 256×256 pixels at 30m resolution. We remove grid cells that have no or nearly no forest cover, then randomly assign each cell to one of 32 splits: The eight temporal splits (seven years plus one portion reserved for future years), crossed

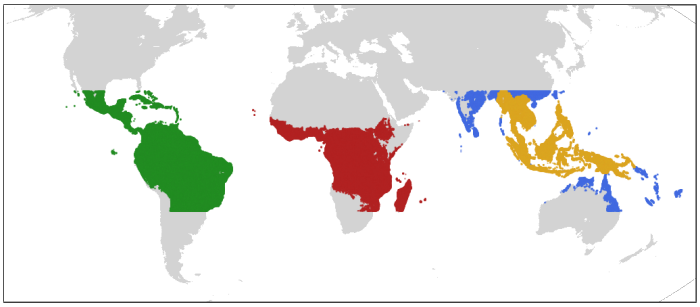

Figure 2: The study region covers the forested areas of the tropics. Shown are the locations of all sampled points, with each regional split highlighted in a different color.

Table 2: The number of samples in each dataset split.

Year	America	Africa	Southeast Asia	Asia-Pacific (other)	Total
2017	32065	21804	11052	4492	69413
2018	31918	21660	10889	4578	69045
2019	32033	21622	10829	4443	68927
2020	31956	21856	11057	4415	69284
2021	31900	21603	10969	4479	68951
2022	31822	21979	10970	4447	69218
2023	31771	21744	10895	4424	68834
Total	255533	174201	87497	35783	553014

with four spatial splits: The continent of America, the continent of Africa, UN-defined Southeast Asia, and the rest of the Asia-Pacific region. We then sample a tile of pixels for each grid cell assigned to a dataset split. This resulted in approximately 0.5M examples, as shown in Table 2.

Each tile consists of a collection of 4D tensors with dimensions *time*, *height*, *width*, and *channels*, that can be ingested by deep learning models. All tiles have a pixel size of 30m and height and width of 7690m (256 pixels), but have varying time and channel dimensions based on the source dataset. Because deforestation happens to only a small fraction of pixels at any one time relative to the total area of forest, the dataset features heavy class imbalance, with an overall proportion of 0.65% of pixels labeled as deforestation.

3.2 MODELS

Random Forest Decision tree

We tested gradient-boosted decision trees using the Yggdrasil Decision Forests (YDF) library (Guillame-Bert et al., 2023). This is a pixel-wise model, operating on each pixel independently.

UNet3D

The UNet3D architecture is an extension of the U-Net convolutional architecture (Ronneberger et al., 2015) to handle temporal features. We follow the architecture used by Rustowicz et al. (2019). U-Net models employ successive stages of downsampling convolution, followed by successive stages of upsampling transposed convolution, all with residual connections between the down and up intermediate layers at each resolution.

U-TAE (U-Net with Lightweight Temporal Attention)

The U-TAE architecture (Garnot & Landrieu, 2021) was initially developed for crop segmentation, for which it was recently state of the art. It combines convolution for spatial processing with self attention for temporal processing. The self-attention collapses the temporal dimension at the bottom-most, or most coarse level of the U-Net. The architecture employs a simplified attention mechanism that was shown to increase speed while sacrificing little to no performance (Garnot & Landrieu, 2020).

TSViT (Temporal-Spatial Vision Transformer)

The TSViT model (Tarasiou et al., 2023) is an extension of the original vision transformer model (Dosovitskiy et al., 2020), which employs self-attention transformers applied to image patches to perform vision tasks. The TSViT model adapts the ViT architecture for satellite image time series by factorizing the transformer encoder into self-attention blocks that sequentially process the temporal and then spatial dimensions.

It further introduces multiple learnable class tokens (one per class) and acquisition-time-specific temporal positional encodings to handle irregularly sampled data.

MTSViT (Multimodal Temporal-Spatial Vision Transformer)

The MTSViT model (Jiang & Neumann, 2025) extends the TSViT by adapting its architecture to process information from multiple input modalities which may have heterogeneous characteristics (e.g., optical, radar). The MTSViT can tokenize multiple inputs, each with potentially different patch sizes corresponding to varying spatial or temporal resolutions. It also adds a cross-attention-based transformer decoder, inspired by DETR (Carion et al., 2020), which follows the modality encoders and that fuses token representations. In contrast to TSViT, whose decoder heads project encoded features directly to task outputs, the MTSViT performs transformer-based multi-modal fusion: it uses tokens from a chosen primary modality (e.g. Sentinel-2 imagery) as queries, which attend to tokens from the other modalities (acting as keys and values) via cross-attention, enabling the model to learn and integrate multimodal information. For this work, we have extended the original MTSViT from Jiang & Neumann (2025) to allow greater architectural flexibility through options for: processing spatial features before temporal, or vice-versa; separate spatial and temporal encoders, enabling each modality to be processed by a dedicated stream before fusion; and separate decoders, allowing query tokens to attend to each modality's tokens independently before fusing the results.

3.3 Training

3.3.1 Data preprocessing

Table 1 shows the preprocessing steps applied to each data source. For each data source, we normalized the values to have a mean of 0 and standard deviation of 1 (either roughly or exactly), except for binary layers which we left as (0, 1). Data sources with long-tailed values such as Sentinel-2 imagery and population were log-transformed.

For the Random Forest model, we first performed all of the preprocessing required for the deep learning models, then, for Sentinel-2 imagery, we composited the timeseries into a cloud-free mean as described in Table 1, and for a given pixel, we computed for each feature a vector consisting of the mean, standard deviation, variance, and each 10th-percentile over the 63×63 patch centered on that pixel. To limit dataset size, we extracted patches centered on pixels arranged over a regular grid of spacing 31×31. This results in a dataset containing fewer pixels than the tile-based models, but this reflects the fundamental difference between the two approaches: tabular-style models like Decision Trees use features that are engineered to be informative about the phenomenon of interest, and thus typically carry more information (such as the median luminance of a patch of pixels) than the raw features used in deep learning models (such as the luminance of a single pixel).

3.3.2 Hyperparameters

Table 3 shows the model configuration parameters used for training each model.

All deep learning models were trained on Google TPUv4 with SGD with Nesterov acceleration (Nesterov, 1983; Sutskever et al., 2013) momentum of 0.9, gradient norm clipping of 1.0 (Pascanu et al., 2012), and a cosine weight decay schedule (Loshchilov & Hutter, 2016).

For all models, we tuned hyperparameters using all data (satellite imagery, auxiliary layers, and change history) for the 2023 split, which has the most historical data and is closest in time to the present, so we would expect its dynamics to be most similar to today's. For all deep learning models, we swept over learning rate, batch size, weight decay, gradient clipping norm, number of warm-up epochs, and total number of epochs, and we found that a learning rate of 0.3, batch size of 512 (except for the MTSViT, where a batch size of 128 was optimal), and weight decay of 1.0×10^{-4}, gradient clipping norm of 1.0, 1 warm-up epoch, and 16 total epochs were optimal (or among several equivalently optimal values).

We also compared binary cross entropy loss with several variants of Dice loss, but mainly Tanimoto Dice loss with complement (Diakogiannis et al., 2019) which we found to work the best among Dice loss variants. We swept over several ratios of weight between the two, ranging from fully cross entropy to fully Dice loss. We found that all models performed best with full cross entropy loss.

Table 3: Model and training hyperparameters.

model	**parameters**
Random Forest	num trees = 20
UNet3D	feature dimension = 8
U-TAE	attention heads = 8 model dimension = 128 k = 16 encoder widths = [64, 64, 64, 128] decoder widths = [32, 32, 64, 128]
TSViT	head dimension = 64 num heads = 4 patch size = 4×4 spatial depth = 4 temporal depth = 4 width = 192
MTSViT	separate decoders = True separate temporal encoders = True processing order = temporal → spatial head dimension = 64 num heads = 4 patch size = 4 spatial depth = 2 temporal depth = 2 width = 256

We also experimented with a weighted loss function to address the heavy class imbalance, but we found that this did not perform any better than the standard equal weight per class.

Finally, for each model, we swept over model-specific parameters using the Southeast Asia subset of the data, finding the values listed in Table 3 to be optimal (or among several equivalently optimal values). For the MTSViT, we found that the most important hyperparameters were separate spatial and temporal decoders, and a processing order of temporal followed by spatial. For experiments on the full dataset, we repeated the hyperparameter sweep for the MTSViT and found the optimal values to be unchanged.

For the Random Forest model, we used the default parameters for the YDF gradient-boosted learner model except with numerical discretization which dramatically speeds up training with minimal effect on accuracy. We swept over patch size, grid spacing, and the number of trees, and found that a patch size of 63, grid spacing of 31, and 20 trees performed best.

4 Results

We carried out our experiments in two stages: in the first, we aimed to test which models from the literature perform best, with an emphasis on deep-learning based models versus classical machine learning. In this stage, we restricted our dataset to just the subset covering Southeast Asia. This allowed us to more quickly iterate, while retaining a scale large enough to still include entire countries. In the second stage, following our learnings in stage 1, we test the most promising model on an expanded spatial scope that includes the entire tropics.

We measured Area Under the ROC Curve (ROC-AUC) for per-pixel classification and Pearson correlation with the proportion of deforestation over an entire tile. ROC-AUC measures the tradeoff between false

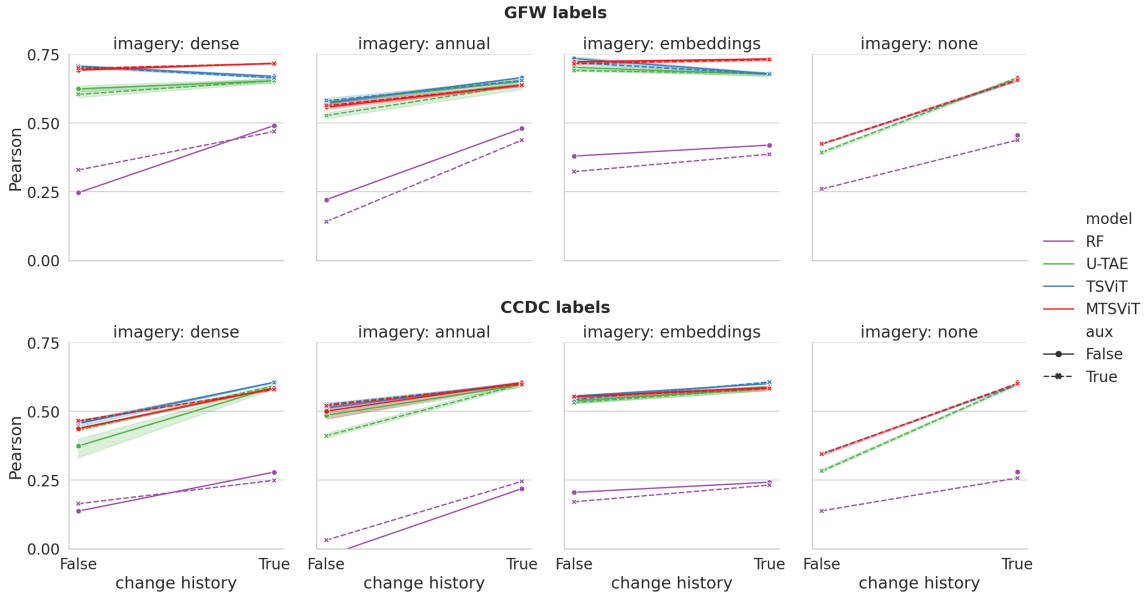

(a) Tile-wise Pearson correlation

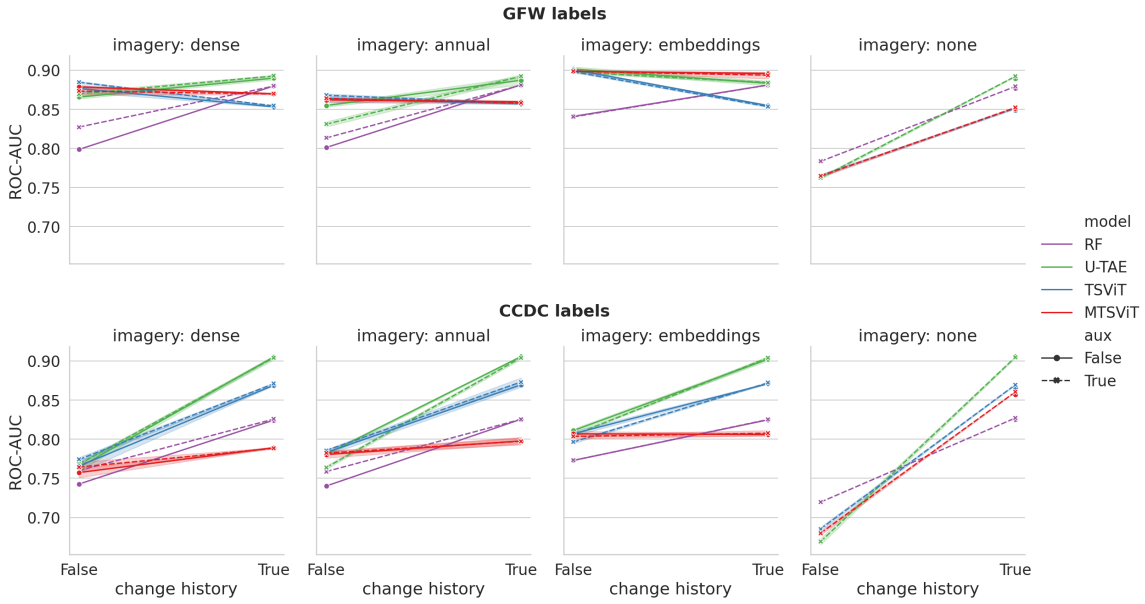

(b) ROC-AUC

Figure 3: Metrics for all ablation conditions for Southeast Asia as a function of the presence/absence of the change-history layer (mean over 5 seeds, rounded to 2 decimal places, with shaded area showing the 95% confidence interval, except for the Random Forest (RF) model, whose training is deterministic). For visual clarity, the results for UNet3D are not shown, as they had high variance and were generally lower than those of the other deep learning models, however scores for that model can be found in Appendix A.

positives and false negatives as the decision threshold is varied. Tile-level Pearson correlation measures the linear relationship between the mean probability of deforestation over the entire tile compared to the proportion of pixels actually deforested.

We found that the pattern of performance differed according to the label source and metric, suggesting that some models may be better at classifying individual pixels (as measured by ROC-AUC), while other models may be better at broadly predicting the amount of deforestation in a given area (as measured by the tile-level correlation). We believe that tile-level correlation probably accords better with downstream use-cases, as users will most likely care about deforestation patterns at scales much coarser than 30m. Therefore, the second stage of experiments covering the entire tropics, we focus on models that achieve the best tile-level Pearson correlation.

Importantly, we compute metrics for all pixels in a tile, in contrast to Ball et al. (2022), who computed metrics over only the single central pixel of each tile. Whole-tile metrics are important because performing inference (i.e. map-making) with deep learning models requires stitching together tiles rather than pixels, otherwise it would require an entire inference pass per pixel, which would be prohibitively slow and costly. For example, rendering a map that uses the central 96×96 pixels of each tile would require nearly 10,000× fewer inference passes than if we rendered pixel-by-pixel. Therefore it is important that our metrics measure model performance in this context, reflecting how the models will actually be used in practice.

4.1 Southeast Asia

Figure 3a and Table A.1 show tile-level Pearson correlation for all ablation conditions for Southeast Asia. We can observe several patterns from these results. First, the MTSViT model performs the best on average, except for when predicting CCDC labels as measured by ROC-AUC. Second, the change history layer is important; in most cases, it enables an increase in performance, as seen by the difference in score between the left and right sides of each condition. Third, change history alone is sufficient to achieve good, but not the best scores, as seen by the similarity between the best scores in the "imagery: none" condition as compared to the others. Fourth, in many cases, removing the auxiliary layers actually improves performance, and for the best models they have little effect, as seen by the dotted lines often appearing lower than or nearby their solid counterparts. Fifth, short temporal context is sufficient, as seen by the better scores achieved by the dense Sentinel-2 imagery (1 year) and the satellite embeddings (2 years). Lastly, model performance differs significantly depending on label source, such as lower correlation with the noisier CCDC labels, and smaller, simpler models often outperforming larger, more complex models.

The observation that change history alone is sufficient for good performance is perhaps surprising, but this result underscores previous findings in the literature that the best predictor of future deforestation is proximity to previous deforestation (Rosa et al., 2013). However the change history layer also performs two other significant functions in our dataset. First, the change history provides more than just distance to recent deforestation for a target pixel, instead providing the full spatial and temporal history of deforestation in the whole tile, including, for example, local waves of deforestation – rich information that an expressive deep learning model can be expected to learn to make use of. Second, the change history informs the model about the dynamics and state of the change detection algorithm itself. The models have to not only learn the (implicit) true dynamics of forest change, they also have to learn how those dynamics are captured and represented by the algorithm that generates the labels. Particularly, the change history allows the model to understand the "state" of the detection algorithm at the time of prediction, for example whether a particular pixel has already been classified as changed in a previous year, which we might expect to be highly useful for reducing noise and error in the predictions.

Figure 4 shows several risk forecast maps for models trained on Southeast Asia. These were generated by running inference over a regular grid of 2.88km×2.88km (i.e. keeping the central 96×96 30m pixels of each 224×224 pixel image). We can see that even though the models that generated each forecast all achieve similar scores, they sometimes produce qualitatively different risk predictions. For example, the choice of ground truth labeling algorithm (GFW-GFC versus CCDC), input imagery, and model all impact the output. Particularly notable are the differences resulting from different input imagery. We hypothesize that this is due to additional information present in the embeddings (that were trained on many sources of data including the cloud-piercing Sentinel-1 imagery) that may not be present in the single source of Sentinel-2 imagery. Based

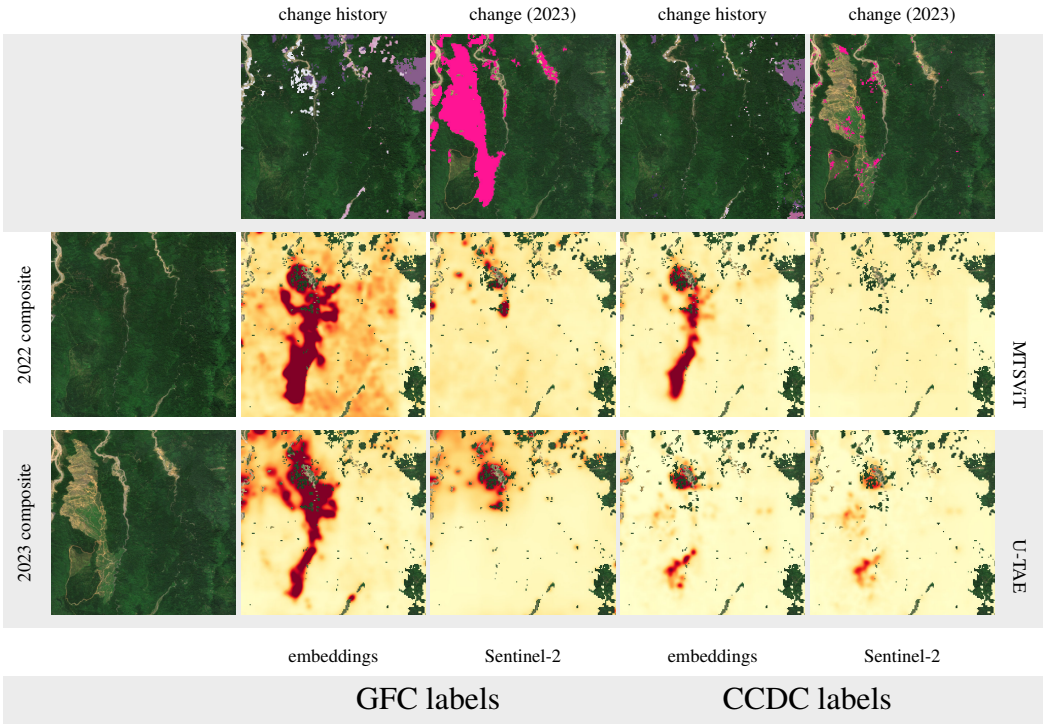

Figure 4: Outputs of models trained on Southeast Asia, varying input imagery, model type, and label source. Each image shows a 5×5km area in northeast Sumatra, Indonesia. The change history images show older change in dark purple progressing to newer change in light purple. The risk forecasts are for 2023, with non-forest or previously deforested area (according to GFC) masked out (and thus showing the background imagery). Light yellow represents lower relative risk and red represents higher relative risk. All models were trained with change history, but without auxiliary layers.

on these results, we advise that the choice of model be informed by the requirements of the particular use case.

4.2 Pan-tropical

Following the initial experiments on the subset of the data in Southeast Asia, we then focused on applying our learnings to maximize performance on the entirety of the tropics. We focused on the best performing model on GFW-GFC labels from the previous set of experiments, the MTSViT model using embeddings with change history. We first repeated the hyperparameter sweep and verified that the optimal training settings were unchanged when using the larger, pan-tropical dataset. We obtained tile-wise Pearson correlation of 0.62 and ROC-AUC of 0.90.

That Pearson correlation is significantly lower when training on the entire tropics than when training on Southeast Asia alone suggests that deforestation dynamics may differ across regions. To investigate this, we trained and evaluated on sub-regions individually to understand the variance between regions and to find out whether training on individual regions was superior to pan-tropical training. Table 4 shows Pearson correlation for models trained on either individual sub-regions or the entire tropics, and then evaluated on those individual regions. We can see that training on the entire tropics gives nearly equivalent scores to training on each region individually, and also the America region clearly stands out as having lower correlation. This suggests that deforestation dynamics in this region are harder to forecast (in 2023), perhaps due to political or regulatory changes in that region that render data from previous years less informative than in other regions, or possibly due to increased prevalence of harder-to-predict drivers of deforestation such as fire.

	Pan-tropical	America	Africa	Southeast Asia	Asia-Pacific
Pan-tropical	.62	.47	.76	.74	.69
Individual		.44	.76	.73	.70

Table 4: Tile-wise Pearson correlation for the MTSViT model when trained on either the entire dataset or on individual regions and evaluated on individual regions.

5 Discussion

5.1 Responsible use

Deforestation risk forecasting models aim to advance scientific understanding, protect biodiversity, enable proactive forest management, and inform global industry standards. As with any research, the responsible development and deployment of such models raises ethical and societal considerations. Here, we focus on two categories of pre-deployment considerations concretely associated with our model, namely, having to do with information *flattening*, as well as risks arising from potential model inaccuracies.

First, as proposed by Francês & Ricci (2020), relying primarily on remote sensing data risks a general *flattening* of knowledge and information, including in the context of deforestation. By relying on measurements conducted from space, there is the potential for losing critical pieces of local context, including important social, cultural, and political nuances that influence deforestation patterns. For instance, a model may accurately predict that rainforests managed by Indigenous peoples have low risk of deforestation without, however, reflecting that such a low risk is the result of those communities' successful efforts at warding off deforestation (Sze et al., 2021). This means that even technically accurate, high-level prediction methods may lead to oversimplified understandings of complex local dynamics, in this instance potentially undermining the effectiveness of Indigenous Peoples' conservation efforts. Similarly, failing to integrate deforestation risk with biodiversity indices might result in neglecting areas of high ecological importance, which underscores the need for a more holistic approach that combines deforestation risk assessments with comprehensive biodiversity data. It is particularly important to be aware of risks associated with information "flattening" if we consider that policy recommendations may be developed on the back of deforestation predictions.

A second category of ethical risks relates to potential mishandling of inevitable inaccurate predictions, i.e. false negatives and false positives. In this context, false negatives are cases where a model inaccurately predicts that a given area is not at risk of deforestation, potentially resulting in less protection or management of a genuinely at-risk area. Here, we can draw an analogy to fisheries prediction models, where recent evidence suggests that widespread overestimation of fish stocks may have contributed to systemic overfishing and, by extension, to global stock collapse (Edgar et al., 2024). Conversely, false positives, or cases where the model predicts high risk where it should not be, may incur undue scrutiny or otherwise negatively affect landowners, particularly smallholders who may lack the capacity or economic influence to counter claims of deforestation risk.

While using deforestation predictions carries risk, we believe that these risks can be mitigated in several ways, with responsibility jointly falling across all stakeholders involved in producing, deploying, and using such forecasts. For researchers, it is important to not only make prediction models as accurate as possible, but to also characterize how well they perform and to what extent and in what situations they can be relied upon. For deployers, such as those who are hosting model outputs and providing data to users, open source and open access creates a level playing field for information access that allows all stakeholders from governments to commercial actors to NGOs to landowners to participate in risk-informed decisions. Finally, for users it is important that deforestation predictions are used as just one element of a more holistic, human-driven decision making process that is grounded on a range of evidence and contextual information, including but not limited to deforestation predictions.

5.2 Limitations and Future Work

We have presented the ForestCast dataset, the first dataset dedicated to training deep learning models for the task of deforestation risk prediction. Our study demonstrates that deep learning models can accurately forecast deforestation risk, and that they can even do so with only minimal data, namely a single layer summarizing the past history of forest change, or a single annualized embedding from a geo-foundational model. It also reveals several limitations and avenues for refinement.

First, despite leveraging an extensive historical record of satellite imagery, our analysis is inherently constrained by data availability and quality. Space-based observations inherently cannot account for crucial predictive factors such as political and legal frameworks. Furthermore, the accuracy of our predictions is contingent upon the quality of the ground-truth data, which, in our case, is algorithmically generated. Consequently, the curation and accuracy of deforestation labels represents a significant opportunity for improvement. Towards this end, recent improvements in delineating natural forests from other types of forest (Neumann et al., 2025) and understanding the drivers of deforestation (Sims et al., 2025) seem promising.

Related to data is the fact that deforestation is a dynamic, non-stationary process, where the relationship between predictive variables and deforestation patterns evolves over time due to factors like political shifts, regulatory changes, economic pressures, and societal attitudes. Future research should explore the integration of temporal data reflecting these variables, alongside the spatial features traditionally used in such studies.

Additionally, it is not clear how well the metrics we (and others) use map onto real-world use cases and outcomes. For example, how much real-world deforestation would be mitigated by a model that achieves 0.1 better Pearson correlation? Further work is required to assess the relationship between the metrics that we are able to measure and the outcomes that users care about, or whether there may even be additional metrics that are more informative about real-world effectiveness.

Lastly, to make deforestation risk models truly useful, they must be reliable and trustworthy. As discussed in Section 5.1, beyond mere accuracy, these models should characterize when, where, and how accurate they are. Incorporating calibrated uncertainty estimates and explainability techniques are promising directions for future exploration, that would enhance the transparency and utility of these models.

REFERENCES

James G C Ball, Katerina Petrova, David A Coomes, and Seth Flaxman. Using deep convolutional neural networks to forecast spatial patterns of amazonian deforestation. *Methods Ecol. Evol.*, 13(11):2622–2634, November 2022. ISSN 2041-210X. doi: 10.1111/2041-210x.13953. URL https://besjournals.onlinelibrary.wiley.com/doi/10.1111/2041-210X.13953.

Nikolaos Ioannis Bountos, Arthur Ouaknine, and David Rolnick. FoMo-bench: a multi-modal, multi-scale and multi-task forest monitoring benchmark for remote sensing foundation models. *arXiv [cs.CV]*, 15 December 2023. URL http://arxiv.org/abs/2312.10114.

Christopher F Brown, Michal R Kazmierski, Valerie J Pasquarella, William J Rucklidge, Masha Samsikova, Chenhui Zhang, Evan Shelhamer, Estefania Lahera, Olivia Wiles, Simon Ilyushchenko, Noel Gorelick, Lihui Lydia Zhang, Sophia Alj, Emily Schechter, Sean Askay, Oliver Guinan, Rebecca Moore, Alexis Boukouvalas, and Pushmeet Kohli. AlphaEarth foundations: An embedding field model for accurate and efficient global mapping from sparse label data. *arXiv [cs.CV]*, 8 September 2025. doi: 10.48550/arXiv.2507.22291. URL http://arxiv.org/abs/2507.22291.

Nicolas Carion, Francisco Massa, Gabriel Synnaeve, Nicolas Usunier, Alexander Kirillov, and Sergey Zagoruyko. End-to-end object detection with transformers. *arXiv [cs.CV]*, 26 May 2020. doi: 10.48550/arXiv.2005.12872. URL http://arxiv.org/abs/2005.12872.

CIESIN. Gridded population of the world, version 4 (gpwv4): Population density, revision 11, 2017. URL http://dx.doi.org/10.7927/H49C6VHW.

Copernicus. Sentinel data, 2025.

Gretchen C Daily, Susan Alexander, Paul R Ehrlich, Larry Goulder, Jane Lubchenco, Pamela A Matson, Harold A Mooney, Sandra Postel, Stephen H Schneider, David Tilman, and George M Woodwell. Benefits supplied to human societies by natural ecosystems. *Issues Ecol.*, (2), 1997. ISSN 1092-8987. URL https://www.esa.org/wp-content/uploads/2013/03/issue2.pdf.

Foivos I Diakogiannis, François Waldner, Peter Caccetta, and Chen Wu. ResUNet-a: a deep learning framework for semantic segmentation of remotely sensed data. *arXiv [cs.CV]*, 1 April 2019. URL http://arxiv.org/abs/1904.00592.

Alexey Dosovitskiy, Lucas Beyer, Alexander Kolesnikov, Dirk Weissenborn, Xiaohua Zhai, Thomas Unterthiner, Mostafa Dehghani, Matthias Minderer, Georg Heigold, Sylvain Gelly, Jakob Uszkoreit, and Neil Houlsby. An image is worth 16x16 words: Transformers for image recognition at scale. *arXiv [cs.CV]*, 22 October 2020. URL http://arxiv.org/abs/2010.11929.

J R Eastman and J Toledano. A short presentation of the land change modeler (LCM). In *Geomatic Approaches for Modeling Land Change Scenarios*, Lecture notes in geoinformation and cartography, pp. 499–505. Springer International Publishing, Cham, 2018. ISBN 9783319608006,9783319608013. doi: 10.1007/978-3-319-60801-3_36. URL https://scholar.google.com/citations?view_op=view_citation&hl=en&citation_for_view=JrGeWbYAAAAJ:K3LRdlH-MEoC.

Graham J Edgar, Amanda E Bates, Nils C Krueck, Susan C Baker, Rick D Stuart-Smith, and Christopher J Brown. Stock assessment models overstate sustainability of the world's fisheries. *Science*, 385(6711): 860–865, 23 August 2024. ISSN 0036-8075,1095-9203. doi: 10.1126/science.adl6282. URL https://www.science.org/doi/10.1126/science.adl6282.

Tim Engelmann and Malte Toetzke. Can deep learning help to forecast deforestation in the amazonian rainforest? In *NeurIPS 2023 Workshop on Tackling Climate Change with Machine Learning*. Climate Change AI, 16 December 2023. URL https://www.climatechange.ai/papers/neurips2023/22/paper.pdf.

European Commission: Directorate-General for Environment. *EU Deforestation Regulation – An opportunity for smallholder*. Publications Office of the European Union, 2023. doi: 10.2779/9252. URL https://data.europa.eu/doi/10.2779/9252.

European Union. Regulation (EU) 2023/1115 of the European Parliament and of the Council of 31 May 2023 on the making available on the Union market and the export from the Union of certain commodities and products associated with deforestation and forest degradation and repealing Regulation (EU) No 995/2010. Official Journal of the European Union, June 2023. URL https://eur-lex.europa.eu/legal-content/EN/TXT/?uri=CELEX:32023R1115. Accessed: Dec 2024.

Food and Agriculture Organization. *The state of the world's forests 2014: enhancing the socioeconomic benefits from forests*. Food & Agriculture Organization of the United Nations (FAO), Rome, Italy, 30 November 2014. ISBN 9789251082690. URL https://openknowledge.fao.org/handle/20.500.14283/i3710e.

Forest Data Partnership. Palm probability model (community models), 2025.

Diana Francês and Noemi Ricci. Ethical advisory report AN EARLY WARNING SYSTEM FOR EARLY DETECTION AND PREDICTING DEFORESTATION. Technical report, 1 April 2020. URL https://www.researchgate.net/publication/350354148_Ethical_Advisory_Report_AN_EARLY_WARNING_SYSTEM_FOR_EARLY_DETECTION_AND_PREDICTING_DEFORESTATION_Ethical_Advisory_Report_WWF_Netherlands.

Vivien Sainte Fare Garnot and Loic Landrieu. Lightweight temporal self-attention for classifying satellite image time series. *arXiv [cs.CV]*, 1 July 2020. URL http://arxiv.org/abs/2007.00586.

Vivien Sainte Fare Garnot and Loic Landrieu. Panoptic segmentation of satellite image time series with convolutional temporal attention networks. *arXiv [cs.CV]*, 16 July 2021. URL http://arxiv.org/abs/2107.07933.

Elizabeth Goldman, Nancy Harris, and Thomas Maschler. Predicting future forest loss in the democratic republic of the congo's carpe landscapes. https://files.wri.org/d8/s3fs-public/predicting-future-forest-loss-democratic-republic-congos-carpe-landscapes_0.pdf. Accessed: 2022-9-1.

Noel Gorelick, Matt Hancher, Mike Dixon, Simon Ilyushchenko, David Thau, and Rebecca Moore. Google earth engine: Planetary-scale geospatial analysis for everyone. *Remote Sensing of Environment*, 2017. doi: 10.1016/j.rse.2017.06.031. URL https://doi.org/10.1016/j.rse.2017.06.031.

Noel Gorelick, Zhiqiang Yang, Paulo Arévalo, Eric L Bullock, Katherin Patricia Insfrán, and Sean P Healey. A global time series dataset to facilitate forest greenhouse gas reporting. *Environ. Res. Lett.*, 18(8):084001, 1 August 2023. ISSN 1748-9326. doi: 10.1088/1748-9326/ace2da. URL https://iopscience.iop.org/article/10.1088/1748-9326/ace2da/meta.

Mathieu Guillame-Bert, Sebastian Bruch, Richard Stotz, and Jan Pfeifer. Yggdrasil decision forests: A fast and extensible decision forests library. In *Proceedings of the 29th ACM SIGKDD Conference on Knowledge Discovery and Data Mining, KDD 2023, Long Beach, CA, USA, August 6-10, 2023*, pp. 4068–4077, 2023. doi: 10.1145/3580305.3599933. URL https://doi.org/10.1145/3580305.3599933.

M C Hansen, P V Potapov, R Moore, M Hancher, S A Turubanova, A Tyukavina, D Thau, S V Stehman, S J Goetz, T R Loveland, A Kommareddy, A Egorov, L Chini, C O Justice, and J R G Townshend. High-resolution global maps of 21st-century forest cover change. *Science*, 342(6160):850–853, 15 November 2013. ISSN 0036-8075,1095-9203. doi: 10.1126/science.1244693. URL http://dx.doi.org/10.1126/science.1244693.

Michael Holder. BlackRock steps up investor pressure on its portfolio polluters. https://trellis.net/article/blackrock-steps-investor-pressure-its-portfolio-polluters/, 24 February 2021. Accessed: 2024-12-.

IPBES. Global assessment report on biodiversity and ecosystem services of the intergovernmental science-policy platform on biodiversity and ecosystem services, 2019. URL https://zenodo.org/records/6417333.

Rodolfo Jaffé, Samia Nunes, Jorge Filipe Dos Santos, Markus Gastauer, Tereza C Giannini, Wilson Nascimento, Jr, Marcio Sales, Carlos M Souza, Pedro W Souza-Filho, and Robert J Fletcher. Forecasting deforestation in the brazilian amazon to prioritize conservation efforts. *Environ. Res. Lett.*, 16(8):084034, 29 July 2021. ISSN 1748-9326. doi: 10.1088/1748-9326/ac146a. URL https://iopscience.iop.org/article/10.1088/1748-9326/ac146a/meta.

Yuchang Jiang and Maxim Neumann. Not every tree is a forest: Benchmarking FORest TYpes from satellite remote sensing. *arXiv [cs.CV]*, 3 May 2025. doi: 10.48550/arXiv.2505.01805. URL http://arxiv.org/abs/2505.01805.

Alexandre Lacoste, Nils Lehmann, Pau Rodriguez, Evan David Sherwin, Hannah Kerner, Björn Lütjens, Jeremy Andrew Irvin, David Dao, Hamed Alemohammad, Alexandre Drouin, Mehmet Gunturkun, Gabriel Huang, David Vazquez, Dava Newman, Yoshua Bengio, Stefano Ermon, and Xiao Xiang Zhu. GEO-bench: Toward foundation models for earth monitoring. *arXiv [cs.LG]*, 6 June 2023. URL http://arxiv.org/abs/2306.03831.

Ilya Loshchilov and Frank Hutter. SGDR: Stochastic gradient descent with warm restarts. *arXiv [cs.LG]*, 13 August 2016. doi: 10.48550/arXiv.1608.03983. URL http://arxiv.org/abs/1608.03983.

Johan R Meijer, Mark A J Huijbregts, Kees C G J Schotten, and Aafke M Schipper. Global patterns of current and future road infrastructure. *Environ. Res. Lett.*, 13(6):064006, 1 June 2018. ISSN 1748-9326. doi: 10.1088/1748-9326/aabd42. URL http://dx.doi.org/10.1088/1748-9326/aabd42.

NASA JPL. NASADEM merged DEM global 1 arc second, 2020. URL http://dx.doi.org/10.5067/MEaSUREs/NASADEM/NASADEM_HGT.001.

National Institute For Space Research. Deforestation – legal amazon. URL https://terrabrasilis.dpi.inpe.br/downloads/.

Yurii Nesterov. A method for unconstrained convex minimization problem with the rate of convergence o(1/k2). *Doklady Akademii Nauk Sssr*, 269(3):543–547, 1983.

Maxim Neumann, Anton Raichuk, Radost Stanimirova, Michelle Sims, Sarah Carter, Elizabeth Goldman, Melanie Rey, Yuchang Jiang, Keith Anderson, Petra Poklukar, Katelyn Tarrio, Myroslava Lesiv, Steffen Fritz, Nicholas Clinton, Charlotte Stanton, Dan Morris, and Drew Purves. Natural forests of the world - a 2020 baseline for deforestation and degradation monitoring. https://eartharxiv.org/repository/view/9085/, 29 April 2025. Accessed: 2025-10-30.

Razvan Pascanu, Tomas Mikolov, and Yoshua Bengio. On the difficulty of training recurrent neural networks. *arXiv [cs.LG]*, 21 November 2012. doi: 10.48550/arXiv.1211.5063. URL http://arxiv.org/abs/1211.5063.

Valerie J Pasquarella, Christopher F Brown, Wanda Czerwinski, and W Rucklidge. Comprehensive quality assessment of optical satellite imagery using weakly supervised video learning. *2023 IEEE/CVF Conference on Computer Vision and Pattern Recognition Workshops (CVPRW)*, pp. 2125–2135, 1 June 2023. doi: 10.1109/CVPRW59228.2023.00206. URL https://openaccess.thecvf.com/content/CVPR2023W/EarthVision/papers/Pasquarella_Comprehensive_Quality_Assessment_of_Optical_Satellite_Imagery_Using_Weakly_Supervised_CVPRW_2023_paper.pdf.

Olaf Ronneberger, Philipp Fischer, and Thomas Brox. U-net: Convolutional networks for biomedical image segmentation. In Nassir Navab, Joachim Hornegger, William M Wells, and Alejandro F Frangi (eds.), *Medical Image Computing and Computer-Assisted Intervention – MICCAI 2015*, pp. 234–241, Cham, 2015. Springer International Publishing. ISBN 9783319245744.

Isabel M D Rosa, Drew Purves, Carlos Souza, Jr, and Robert M Ewers. Predictive modelling of contagious deforestation in the brazilian amazon. *PLoS One*, 8(10):e77231, 18 October 2013. ISSN 1932-6203. doi: 10.1371/journal.pone.0077231. URL http://dx.doi.org/10.1371/journal.pone.0077231.

Samapriya Roy, Tyson Swetnam, and Andrew Saah. Samapriya/awesome-gee-community-datasets: Community catalog, 2024. URL https://zenodo.org/records/14042069.

Rose Rustowicz, Robin Cheong, Lijing Wang, Stefano Ermon, M Burke, and D Lobell. Semantic segmentation of crop type in africa: A novel dataset and analysis of deep learning methods. In *Proceedings of the IEEE/CVF Conference on Computer Vision and Pattern Recognition (CVPR) Workshops*, pp. 75–82, 2019. URL https://openaccess.thecvf.com/content_CVPRW_2019/html/cv4gc/Rustowicz_Semantic_Segmentation_of_Crop_Type_in_Africa_A_Novel_Dataset_CVPRW_2019_paper.html.

Marcio Sales, Sytze de Bruin, Martin Herold, Phaedon Kyriakidis, and Carlos Souza, Jr. A spatiotemporal geostatistical hurdle model approach for short-term deforestation prediction. *Spatial Statistics*, 21:304–318, 1 August 2017. ISSN 2211-6753. doi: 10.1016/j.spasta.2017.06.003. URL https://www.sciencedirect.com/science/article/pii/S221167531730163X.

Satelligence. Scaling the forest loss risk index (FLRI) approach across landscapes. Technical report, 23 May 2022. URL https://satelligence.com/wp-content/uploads/2024/02/FLRI-olam.pdf.

Tarek Sboui, Salwa Saidi, and Ahmed Lakti. A machine-learning-based approach to predict deforestation related to oil palm: Conceptual framework and experimental evaluation. *Appl. Sci. (Basel)*, 13(3):1772, 30 January 2023. ISSN 2076-3417,2076-3417. doi: 10.3390/app13031772. URL https://www.mdpi.com/2076-3417/13/3/1772.

André Schröder. European bill passes to ban imports of deforestation-linked commodities. https://news.mongabay.com/2022/09/european-bill-passes-to-ban-imports-of-deforestation-linked-commodities/, 15 September 2022. Accessed: 2024-12-.

Marc Simard, Lola Fatoyinbo, Charlotte Smetanka, Victor H. Rivera-monroy, Edward Castañeda-Moya, Nathan Thomas, and Tom Van der stocken. Global mangrove distribution, aboveground biomass, and canopy height, 2 May 2019. URL http://dx.doi.org/10.3334/ORNLDAAC/1665.

Marc Simard, Michael Denbina, Charles Marshak, and Maxim Neumann. A Global Evaluation of Radar-Derived Digital Elevation Models: SRTM, NASADEM, and GLO-30. *Journal of Geophysical Research: Biogeosciences*, 129(11):e2023JG007672, 2024. doi: https://doi.org/10.1029/2023JG007672. URL https://agupubs.onlinelibrary.wiley.com/doi/abs/10.1029/2023JG007672. e2023JG007672 2023JG007672.

Michelle J Sims, Radost Stanimirova, Anton Raichuk, Maxim Neumann, Jessica Richter, Forrest Follett, James MacCarthy, Kristine Lister, Christopher Randle, Lindsey Sloat, Elena Esipova, Jaelah Jupiter, Charlotte Stanton, Dan Morris, Christy Melhart Slay, Drew Purves, and Nancy Harris. Global drivers of forest loss at 1 km resolution. *Environ. Res. Lett.*, 20(7):074027, 1 July 2025. ISSN 1748-9326. doi: 10.1088/1748-9326/add606. URL http://dx.doi.org/10.1088/1748-9326/add606.

Carlos M Souza, Jr, Julia Z. Shimbo, Marcos R Rosa, Leandro L Parente, Ane A. Alencar, Bernardo F T Rudorff, Heinrich Hasenack, Marcelo Matsumoto, Laerte G. Ferreira, Pedro W M Souza-Filho, Sergio W de Oliveira, Washington F Rocha, Antônio V Fonseca, Camila B Marques, Cesar G Diniz, Diego Costa, Dyeden Monteiro, Eduardo R Rosa, Eduardo Vélez-Martin, Eliseu J Weber, Felipe E B Lenti, Fernando F Paternost, Frans G C Pareyn, João V Siqueira, José L Viera, Luiz C Ferreira Neto, Marciano M Saraiva, Marcio H Sales, Moises P G Salgado, Rodrigo Vasconcelos, Soltan Galano, Vinicius V Mesquita, and Tasso Azevedo. Reconstructing three decades of land use and land cover changes in brazilian biomes with landsat archive and earth engine. *Remote Sens. (Basel)*, 12(17):2735, 25 August 2020. ISSN 2072-4292,2072-4292. doi: 10.3390/rs12172735. URL https://www.mdpi.com/2072-4292/12/17/2735.

Ilya Sutskever, James Martens, George E Dahl, and Geoffrey E Hinton. On the importance of initialization and momentum in deep learning. In *International conference on machine learning*, pp. 1139–1147, 2013.

Jocelyne S Sze, L Roman Carrasco, Dylan Childs, and David P Edwards. Reduced deforestation and degradation in indigenous lands pan-tropically. *Nat. Sustain.*, 5(2):123–130, 25 November 2021. ISSN 2398-9629,2398-9629. doi: 10.1038/s41893-021-00815-2. URL https://www.nature.com/articles/s41893-021-00815-2.

Michail Tarasiou, Erik Chavez, and Stefanos Zafeiriou. ViTs for SITS: Vision transformers for satellite image time series. *arXiv [cs.CV]*, 12 January 2023. URL http://arxiv.org/abs/2301.04944.

UNEP-WCMC and IUCN. Protected planet: The world database on protected areas (WDPA), 2024. URL www.protectedplanet.net.

Anouk van Stokkom, Jorn Dallinga, Michael Debuyser, Dirk Hoekman, Boris Kooij, Pablo Pacheco, David Thau, Suzanne Valkman, and Hans Beukeboom. An innovative early warning system to tackle illegal deforestation. In *FIG Working Week*, 2020. URL https://www.fig.net/resources/proceedings/fig_proceedings/fig2020/papers/ts06i/TS06I_van_stokkom_dallinga_10667.pdf.

C Vancutsem, F Achard, J-F Pekel, G Vieilledent, S Carboni, D Simonetti, J Gallego, L E O C Aragão, and R Nasi. Long-term (1990-2019) monitoring of forest cover changes in the humid tropics. *Sci Adv*, 7(10), March 2021. ISSN 2375-2548. doi: 10.1126/sciadv.abe1603. URL http://dx.doi.org/10.1126/sciadv.abe1603.

Verra. VM0048 Methodology for Reducing Emissions from Deforestation and Forest Degradation. Technical report, Verra, 2023. URL https://verra.org/methodologies/vm0048-reducing-emissions-from-deforestation-and-forest-degradation-v1-0/. Version 1.0, active since November 27, 2023.

Verra. VMD0055 Estimation of Emission Reductions from Avoiding Unplanned Deforestation. Technical report, Verra, 2024. URL https://verra.org/methodologies/vmd0055-estimation-of-emission-reductions-from-avoiding-unplanned-deforestation-v1-1/ Version 1.1, updated October 21, 2024.

Ghislain Vieilledent, Christelle Vancutsem, Clément Bourgoin, Pierre Ploton, Philippe Verley, and Frédéric Achard. Spatial scenario of tropical deforestation and carbon emissions for the 21st century. *bioRxiv*, pp. 2022.03.22.485306, 12 May 2023. doi: 10.1101/2022.03.22.485306. URL https://www.biorxiv.org/content/10.1101/2022.03.22.485306v3.

Mikaela Weisse, Elizabeth Goldman, and Sarah Carter. Tropical forest loss drops steeply in brazil and colombia, but high rates persist overall. https://research.wri.org/gfr/latest-analysis-deforestation-trends, 4 April 2024. Accessed: 2024-12-.

Xiao Zhang, Liangyun Liu, Tingting Zhao, Xidong Chen, Shangrong Lin, Jinqing Wang, Jun Mi, and Wendi Liu. GWL_FCS30: a global 30 m wetland map with a fine classification system using multi-sourced and time-series remote sensing imagery in 2020. *Earth Syst. Sci. Data*, 15(1):265–293, 17 January 2023. ISSN 1866-3508,1866-3516. doi: 10.5194/essd-15-265-2023. URL https://doi.org/10.5194/essd-15-265-2023.

Zhe Zhu and Curtis E Woodcock. Continuous change detection and classification of land cover using all available landsat data. *Remote Sens. Environ.*, 144:152–171, 25 March 2014. ISSN 0034-4257. doi: 10.1016/j.rse.2014.01.011. URL https://www.sciencedirect.com/science/article/pii/S0034425714000248.

APPENDIX A RESULTS

Table A.1: Tile-wise Pearson correlation for all ablation conditions for Southeast Asia (mean over 5 seeds, rounded to 2 decimal places, except for the Random Forest (RF) model, whose training is deterministic).

				RF	UNet3D	U-TAE	TSViT	MTSViT
label source	imagery	aux	change history					
ccdc	dense	False	False	0.14	0.39	0.37	0.46	0.44
			True	0.28	0.56	0.59	0.61	0.58
		True	False	0.16	0.35	0.43	0.46	0.47
			True	0.25	0.56	0.59	0.61	0.58
	annual	False	False	-0.03	0.40	0.49	0.51	0.50
			True	0.22	0.53	0.60	0.60	0.60
		True	False	0.03	0.39	0.41	0.52	0.52
			True	0.24	0.54	0.60	0.60	0.60
	embeddings	False	False	0.20	0.53	0.54	0.56	0.55
			True	0.24	0.57	0.58	0.60	0.59
		True	False	0.17	0.43	0.53	0.54	0.55
			True	0.23	0.43	0.58	0.61	0.58
	none	False	True	0.28	0.58	0.60	0.60	0.61
		True	False	0.14	0.17	0.28	0.35	0.34
			True	0.26	0.57	0.60	0.60	0.60
gfw	dense	False	False	0.25	0.61	0.62	0.71	0.69
			True	0.49	0.60	0.65	0.67	0.72
		True	False	0.33	0.42	0.60	0.71	0.70
			True	0.47	0.60	0.65	0.66	0.72
	annual	False	False	0.22	0.54	0.58	0.57	0.56
			True	0.48	0.58	0.65	0.67	0.64
		True	False	0.14	0.49	0.53	0.58	0.56
			True	0.44	0.56	0.64	0.65	0.64
	embeddings	False	False	0.38	0.69	0.70	0.73	0.72
			True	0.42	0.59	0.68	0.68	0.73
		True	False	0.32	0.52	0.69	0.72	0.72
			True	0.39	0.45	0.68	0.68	0.73
	none	False	True	0.46	0.62	0.67	0.66	0.66
		True	False	0.26	0.13	0.39	0.42	0.42
			True	0.44	0.62	0.66	0.65	0.66

Table A.2: Area under the ROC curve for all ablation conditions for Southeast Asia (mean over 5 seeds, rounded to 2 decimal places, except for the Random Forest (RF) model, whose training is deterministic).

				RF	UNet3D	U-TAE	TSViT	MTSViT
label source	imagery	aux	change history					
ccdc	dense	False	False	0.74	0.74	0.76	0.77	0.76
			True	0.82	0.88	0.91	0.87	0.79
		True	False	0.76	0.70	0.77	0.77	0.76
			True	0.83	0.88	0.90	0.87	0.79
	annual	False	False	0.74	0.70	0.78	0.78	0.78
			True	0.83	0.87	0.91	0.87	0.80
		True	False	0.76	0.70	0.76	0.79	0.78
			True	0.83	0.88	0.90	0.87	0.80
	embeddings	False	False	0.77	0.79	0.81	0.81	0.81
			True	0.82	0.88	0.90	0.87	0.81
		True	False	0.77	0.75	0.81	0.80	0.80
			True	0.83	0.83	0.90	0.87	0.81
	none	False	True	0.83	0.88	0.91	0.87	0.86
		True	False	0.72	0.59	0.67	0.69	0.68
			True	0.83	0.88	0.90	0.87	0.86
gfw	dense	False	False	0.80	0.83	0.87	0.88	0.88
			True	0.88	0.85	0.89	0.85	0.87
		True	False	0.83	0.76	0.87	0.88	0.87
			True	0.88	0.85	0.89	0.85	0.87
	annual	False	False	0.80	0.82	0.85	0.86	0.86
			True	0.88	0.84	0.89	0.86	0.86
		True	False	0.81	0.80	0.83	0.87	0.86
			True	0.88	0.84	0.89	0.86	0.86
	embeddings	False	False	0.84	0.88	0.90	0.90	0.90
			True	0.88	0.87	0.88	0.85	0.90
		True	False	0.84	0.81	0.90	0.90	0.90
			True	0.88	0.78	0.88	0.85	0.89
	none	False	True	0.88	0.85	0.89	0.85	0.85
		True	False	0.78	0.62	0.76	0.77	0.76
			True	0.88	0.86	0.89	0.85	0.85